Effect of 2,1,3-benzothiadiazole (BTD) dopant on photovoltaic performance improvement of organic solar cells

MAHDI FASIHBEIKI, FARHAD A. BOROUMAND[*]

Department of Electrical Engineering, K.N. Toosi University of Technology, Shariati Street, Tehran, Iran

In this study, 2,1,3-benzothiadiazole (BTD) with different weight ratios (0, 5 and 20 wt %) of the active layer, located between buffer layer and cathode electrode of solar cells, was used to improve the photovoltaic performance of organic solar cells. To clearly evaluate the effect of BTD doping, we have fabricated the active layer with classic low cost (low efficiency) materials. The solar cell structure is poly(ethyleneterephthalate) (PET) / Indium Tin Oxide (ITO) / poly(3,4-ethylenedioxythiophene) : poly(styrenesulfonate) (PEDOT:PSS) / poly[2-methoxy-5-(2-ethylhexyloxy)-1,4-phenylenevinylene] (MEH-PPV) : Fullerene-C_{60} nanoparticles (C_{60}) (2:1) 2,1,3-benzothiadiazole (BTD) / Al. The results show that addition of BTD with 20 wt % of the main active layer had the best effect on the output power of the fabricated solar cells with threefold increase (from 2.8 to 9.0 $\mu W/cm^2$). Additionally, after implementing this method, increase in short circuit current (J_{sc}) was from 0.012 to 0.036 mA/cm^2, while the open circuit voltage (V_{oc}) did not change noticeably. In accordance with analytical models, this study practically suggests that a high mobility dopant such as BTD could be a promising active layer dopant to improve the efficiency of organic solar cells. This efficiency enhancing method is applicable to state of the art organic solar cells.

1. Introduction

Low cost and clean source of energy such as solar energy is highly desirable for the reduction of environmental pollution related with the use of fossil fuels [1]. Silicon-based solar cells have been utilized as an alternative green source of energy, but their cost is still high due to complex production processes [2]. In recent years, the area of organic electronics has been developed rapidly, and vastly been used in many appliances such as high-resolution displays, wearable devices and medical devices. As an alternative to silicon-based devices, organic solar cells are under intensive research due to their unique properties such as ease of processing [3,4], flexibility, tunable properties [5,6] and low cost [7-11].

However, widespread usage of organic solar cells is still limited due to their poor environmental stability and charge transportation across the photoactive layer which causes low efficiency [1]. The photoactive layer of typical bulk-heterojunction solar cells consists of films of conjugated polymers and fullerenes or electron donor/acceptor conjugates. In these photoactive layers, the control over the interpenetrating network is considered as the key step to ensure efficient charge separation/transportation, and the power conversion efficiency is limited by the collection of charges in the electrodes. A reasonable approach to overcome this limitation is by introducing high mobility materials as additives in the active layer of the solar cells. For example, carbon nanotubes were added in organic solar cells to facilitate the charge transportation and improve the power conversion efficiency of the devices [12-14]. Thus, it is

expected that adding other high mobility dopants to the active layer will improve the power conversion efficiency of solar cells. Also, it has been known that ternary blend solar cells may have higher efficiencies due to enhanced light absorption, improved charge separation, carrier transportation, and possible suppressed carrier recombination for the cascade band structure in active layers [12, 15-18].

2,1,3-Benzothiadiazole (BTD) is one of the most important materials used in photoluminescent compounds chemistry. In recent years, many research groups have contributed to development of BTD chemistry and applications [19-25]. This area is expected to grow in following years, especially for solar cells [19, 26-29]. A theoretical study showed that due to existence of two electron-withdrawing imine nitrogen atoms in this unit (C=N), the presence of BTD core is a good factor to improve electron-transporting ability [30].

Thus, due to good electron mobility and some special properties such as low cost, the BTD and its derivatives have been used increasingly in organic light-emitting diodes (OLEDs) [31] and organic thin-film transistors (OTFTs) [32,33] fabrication. Some researchers have used the BTD branched complex molecules as donor in organic solar cells [34], but in contrast we used it in the base form as a high mobility dopant. The BTD has never been reported as an electron transporting small molecule dopant in organic solar cells.

In this research, we have used the BTD in the active layer which is located between the buffer layer and the cathode electrode in solar cells with structure of poly(ethyleneterephthalate) (PET) / Indium Tin Oxide

(ITO)/poly(3,4-ethylenedioxythiophene): poly(styrenesulfonate) (PEDOT:PSS) / poly[2-methoxy-5-(2-ethylhexyloxy)-1,4-phenylenevinylene] (MEH-PPV) : Fullerene-C_{60} nanoparticles (C_{60}) (2:1) 2,1,3-benzothiadiazole (BTD) / Al. This promising strategy of adding high-mobility dopant helped to mitigate the poor charge transportation/collection discussed above and improved the efficiency of solar cells. The operation of fabricated solar cells was analyzed according to the obtained UV-visible absorption spectra of MEH-PPV, C_{60} and BTD and their energy diagram. Then using Atomic Force Microscope (AFM) height images, the effect of BTD addition with different weight ratios (0, 5 and 20 wt %) of the main active layer was investigated on surface roughness. This process was not continued to higher weight ratios, since higher weight ratios might significantly influence the composition of the solar cells. Also, photovoltaic performance of the solar cells was analyzed by comparing the I-V characteristics of the fabricated solar cells. Our experiments also confirm the prediction of solar cell characteristics by analytical models.

In this paper, section 2 describes our proposed structure of the fabricated solar cells, the molecular structures of the organic materials used in the fabrication, and the FT/IR spectra of the organic materials used in active layer. Section 3 contains our fabrication process and section 4 shows the analysis of the solar cells operation. Section 5 presents the conclusion and future research directions.

2. Structure and materials

The structure of the fabricated solar cells is shown in Fig. 1. It consists of inactive PET substrate, ITO anode electrode, PEDOT:PSS buffer layer, MEH-PPV:C_{60} (2:1) BTD active layer and Al cathode electrode. The molecular structures of the organic materials employed in the fabrication of solar cells are shown in Fig. 2. These include BTD (an electron transporting small molecule), C_{60} (a cage-like fused-ring structure made of twenty hexagons and twelve pentagons, with a carbon atom at each vertex of each polygon and a bond along each polygon edge used as a high affinity electron acceptor), MEH-PPV (an electron donor polymer semiconductor) and PEDOT:PSS (a transparent conductive polymer blend with high ductility).
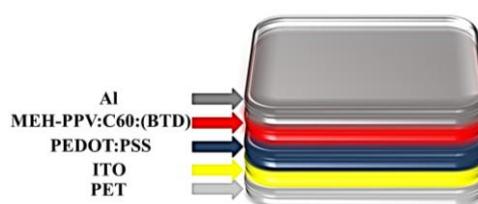
Fig. 1. The structure of the fabricated solar cells comprised of inactive PET substrate, ITO anode electrode, PEDOT:PSS buffer layer, MEH-PPV:C_{60} (2:1) BTD active layer and Al cathode electrode
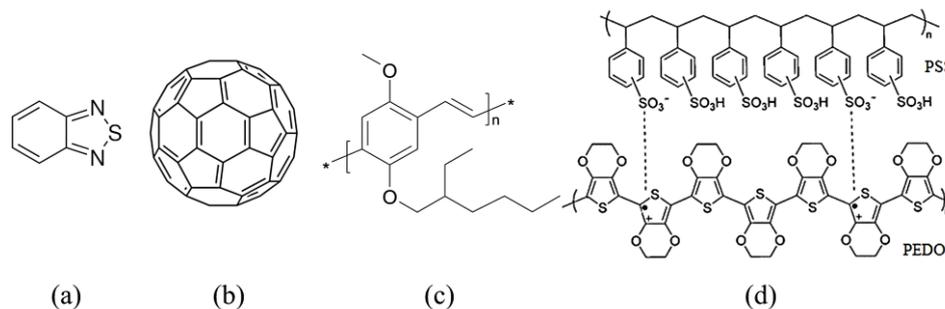
Fig. 2. The molecular structure of (a) BTD, (b) C_{60}, (c) MEH-PPV and (d) PEDOT:PSS

The IR spectrum can be derived from absorption of light exciting molecular vibrations. The positions of absorption bands in the spectrum shows the presence or absence of specific functional groups in a molecule. As a whole, the spectrum constitutes a "fingerprint" which can be used to determine the sample. Fig. 3 shows the FT/IR spectra of MEH-PPV, C_{60} and BTD using a JASCO FT/IR-460 spectrophotometer in the range of 400 to 4000 cm-1. The peaks of our derived spectra are consistent with ones in spectra reported in related works [35-37], means that our materials are in proper conditions.

(a)

(b)

(c)
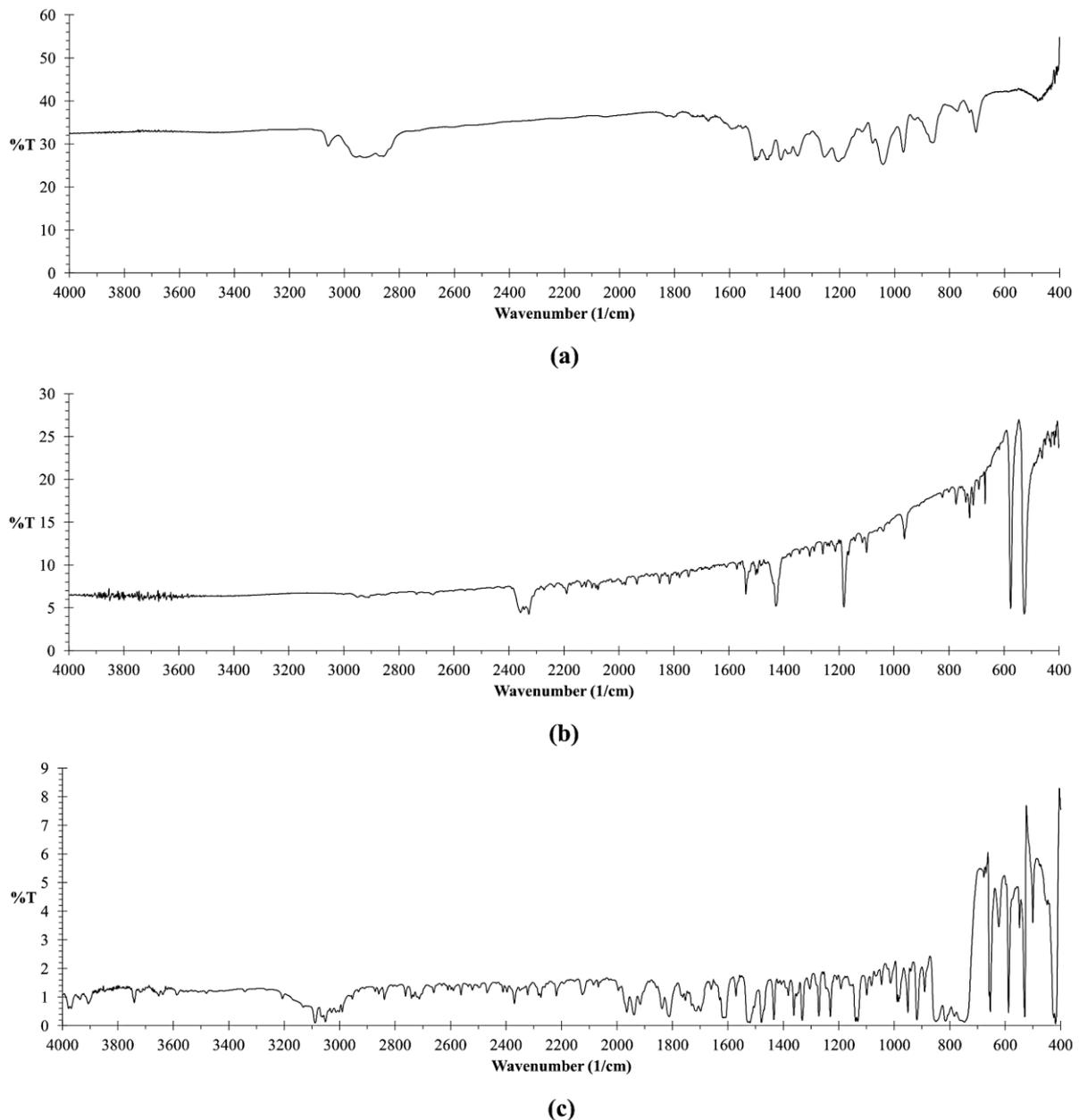
Fig. 3. The FT/IR spectra of (a) MEH-PPV, (b) C$_{60}$ and (c) BTD, which the peaks of spectra are in consistence with peaks in spectra reported in literature [35-37]

3. Experimental

In this section, we describe our method to fabricate the bulk-heterojunction solar cells with BTD dopant. First, a 12 x 12 mm^2 size slice of ITO coated PET (Sigma-Aldrich 639303) sheet was cut and the ribbon stick was used to coat the 12 x 6 mm^2 middle part of ITO coated PET. Then, the ITO substrate was dipped in a solution of HCl : deionized water (DI) (18% v) for one minute to etch the ITO from the edges and prevent the short circuit of the cathode electrode with ITO. Subsequently, the substrate was dipped in acetone until the ribbon stick separated and an ITO strip in 12 x 6 mm^2 size remained on the PET.

Then, the etched ITO was cleaned using an ultrasonic bath and different solvents. At the beginning, the ITO was washed with deionized water and soap at 30°C for 5 minutes, rinsed with deionized water, and subsequently washed with ethanol at 30°C for 5 min. Then, the prepared ITO was dried in oven at 100°C for 60 min. Afterwards, the PEDOT:PSS (1.3% wt dispersion in H2O, conductive grade) (Sigma-Aldrich 483095) was spin-coated at 3000 rpm for 30 seconds and dried in oven at 130°C for 10 minutes, then used as a hole injection/transport layer. The PEDOT:PSS conductive polymer layer improves the hopping ability of holes and reduces the tunneling effect [38]. Also, the spin coating was used for active layer deposition made in the form of bulk-heterojunction by

mixing the donor and acceptor components. The components include the MEH-PPV (Sigma-Aldrich 541443) : Fullerene-C$_{60}$ nanoparticles (Sigma-Aldrich 572500) (2:1) and BTD (Sigma-Aldrich B10900). The BTD is added as a dopant with different weight ratios (0, 5 and 20 wt %) of the main active layer in chlorobenzene as a solvent. The spin-coated layer was dried in oven at 50°C for 5 minutes. Finally, an aluminum (AnalaR BDH Chemicals Ltd Poole England) cathode electrode was coated using the common vacuum thermal evaporation (VTE) method at the pressure of 5 x 10^{-5} torr. After fabrication of the devices, the electrical measurements were done with source measure unit (SMU) (Keithley 238). The fabrication process and measurements were performed at ambient condition without using the glove box or device encapsulation.

A Perkin Elmer Lambda EZ201 spectrophotometer was used to record the absorbance spectra of the components. We have used the Quartz substrates to measure the optical absorption. The morphology and surface properties of the solar cells active layer were analyzed using a Veeco Autoprobe Di CP-II AFM.

4. Results and discussion

UV-visible absorption spectra of MEH-PPV, C$_{60}$ and BTD (the organic materials used in active layer) are measured and shown in Fig. 4. The absorption peaks of composite films are just superposition of MEH-PPV and C$_{60}$ peaks. This means that there is no interaction between two kinds of materials in the ground state [39]. Unlike MEH-PPV which exhibited a strong absorption in the visible range, the C$_{60}$ has exhibited a weak absorption. Thus, the MEH-PPV is the main light absorber.
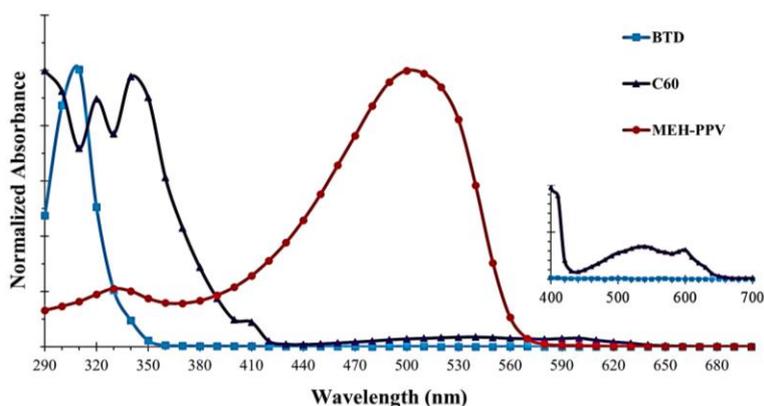
Fig. 4. UV-visible absorption spectra of MEH-PPV, C$_{60}$ and BTD. Unlike MEH-PPV that exhibited a strong absorption in the visible range, the C$_{60}$ has exhibited a weak absorption, indicating that the MEH-PPV is the main light absorber
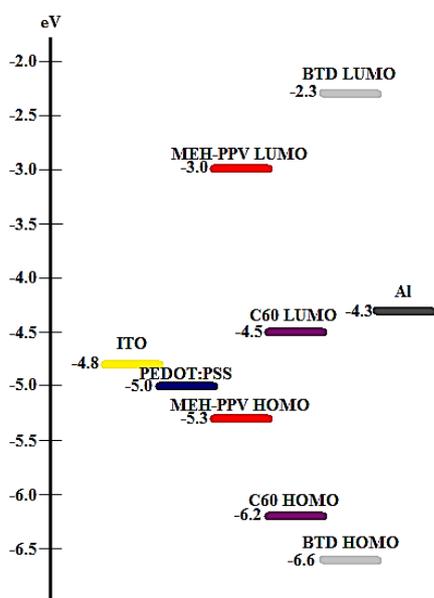
Fig. 5. Energy diagram of the fabricated solar cells showing high energy difference between BTD HOMO/LUMO and other materials energy levels

Energy diagram of the fabricated solar cells is shown in Fig. 5. The high-band gap BTD may only help in exciton (electron-hole pair) dissociation and electron transfer to the cathode electrode.

Morphology of the active layer is known to be a critical factor in the photovoltaic properties of the organic solar cells, as optimal nanoscale-phase-separated domains provides efficient charge extraction and percolates pathways effectively, for charge carrier transportation to the respective electrodes [40]. Fig. 6 shows the AFM height images of the solar cells active layer using BTD with different weight ratios of 0, 5 and 20 wt %. This process was not continued to higher weight ratios, since higher weight ratios might significantly influence the composition of the solar cells. Average roughness and root mean square (RMS) of surface roughness was obtained from the AFM data. RMS is defined as [41]:

$$RMS = \sqrt{\frac{1}{L}\int_0^L |Z^2(x)|\, dx} \qquad (1)$$

where Z(x) denotes the surface profile analyzed in terms of height Z at position x over the evaluation length L of the sample. The results of AFM height images are shown in

Table 1, indicating that the surface roughness of the solar cell active layer decreases with increase in BTD weight ratio. The smoother surface (i.e. more homogeneous morphology) may enhance the charge separation and transportation inside the device, resulting in higher interfacial current. In contrast, the effects of other parameters are negligible. These effects include the increased contact area between the active layer and the cathode electrode (which may result in a more efficient charge collection at the interface) and also internal reflection enhancement (which improves light collection) for the active layers with higher surface roughness [40,42].

(A1)

(A2)

(B1)

(B2)

(C1)

(C2)
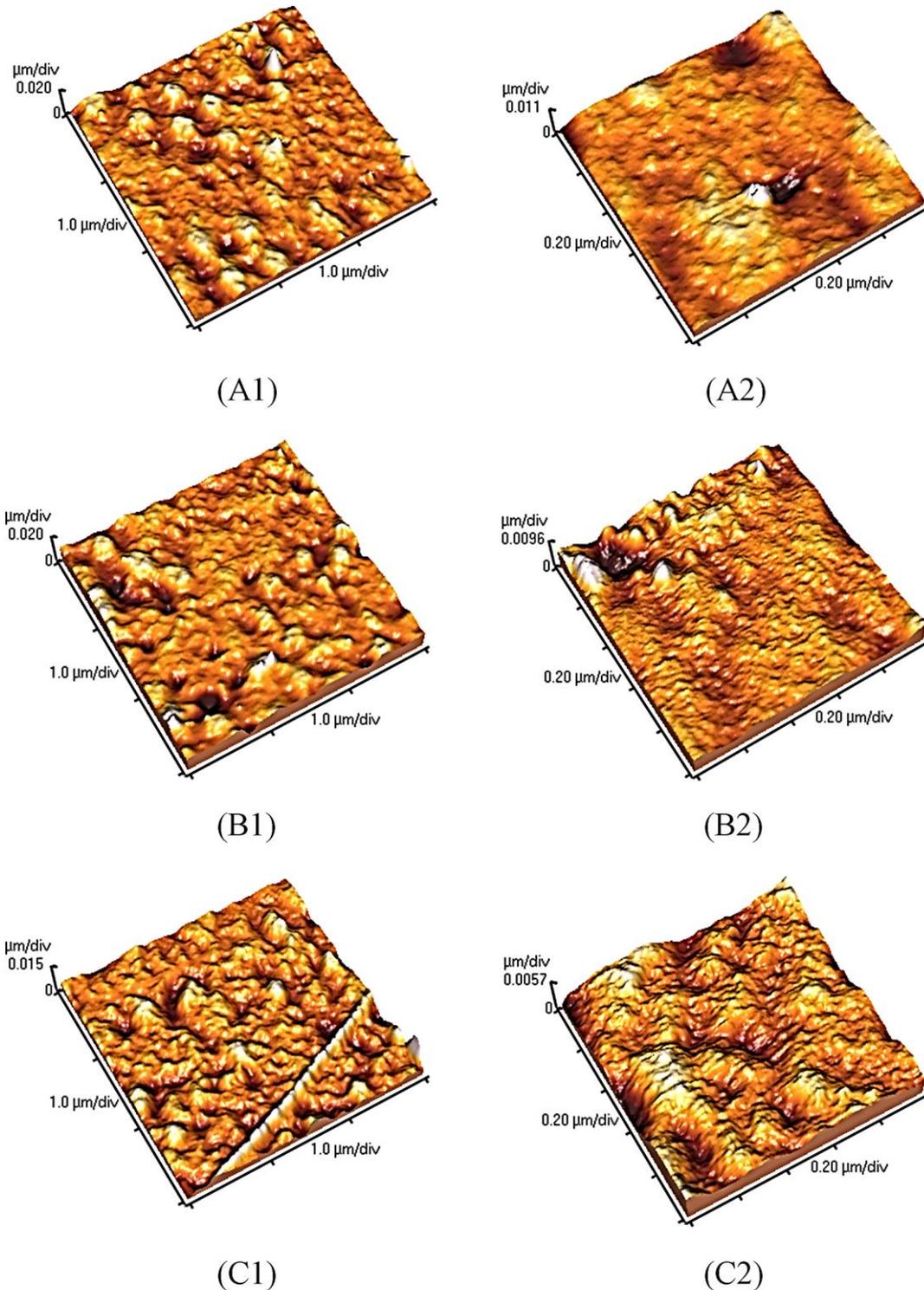
Fig. 6. The AFM height images of the solar cells active layer using BTD with different weight ratios of (a) 0, (b) 5 and (c) 20 wt % in two sizes (3 x 3 and 1 x 1 μm^2) indicating that the surface roughness of the solar cell active layer decreases with increase in BTD weight ratio

Table 1. The AFM height images results of the solar cells active layer

Active Layer	Image	Size	Average Roughness	RMS Roughness
MEH-PPV:C_{60} (2:1)	A1	3 x 3 μm^2	1.103	1.515
	A2	1 x 1 μm^2	0.7302	0.9889
MEH-PPV:C_{60} (2:1) + 5 wt % BTD	B1	3 x 3 μm^2	1.074	1.510
	B2	1 x 1 μm^2	0.6413	0.9081
MEH-PPV:C_{60} (2:1) + 20 wt % BTD	C1	3 x 3 μm^2	1.018	1.360
	C2	1 x 1 μm^2	0.5839	0.7535

Fig. 7 shows the I-V curves of the fabricated solar cells, which were produced using the BTD with different weight ratios (0, 5 and 20 wt %) of the main active layer. The characteristics of the fabricated solar cells are shown in Table 2. The results show that addition of BTD with 20 wt % of the main active layer had the best effect on the maximum output power (P_m) of the fabricated solar cells with threefold increase (from 2.8 to 9.0 $\mu W/cm^2$) (under an ordinary filament lamp). In addition, after BTD doping, the short-circuit current density (J_{sc}) increased from 0.012 to 0.036 mA/cm^2, while the open-circuit voltage (V_{oc}) did not change noticeably.

The UV-visible absorption spectra of BTD (Fig. 4) which is below 350 nm, cannot contribute to photon absorption. So, the observed improvement is not resulted from the optical effect. This may be explained by formation of electron transport subnetworks in the active layer. In a strong electron transport network, all electrons might be transported directly to the cathode electrode via the network and no electron–hole recombination occurs. The high electron mobility of BTD enhances the electron transportation in the active layer by formation of such electron transport subnetworks. This leads to increase in output power and J_{sc} [31].

The positive impact of charge transportation on power conversion efficiency and current-voltage characteristics of organic solar cells is well analytically modeled. It showed an excellent agreement with full drift-diffusion simulations over a wide range of mobilities and illumination intensities, which makes it suitable for realistic efficiency predictions of organic solar cells [43]. The efficiency always increases with the mobility of the charge carriers [44]. In summary, consideration of exciton splitting, recombination, and charge collection all suggest that highly ordered (high mobility) organic materials are more likely to give higher efficiency cells [45].

By addition of BTD with 5 wt % of the main active layer, the recombination rate before charge collection by electrodes decreases due to the enhanced electron transportation. Thus, the Fill Factor of the fabricated solar cells increases. The Fill Factor decreases in slight amount with 20 wt % BTD due to more electron scattering, resulting

in increase of recombination rate before charge collection by electrodes [46].
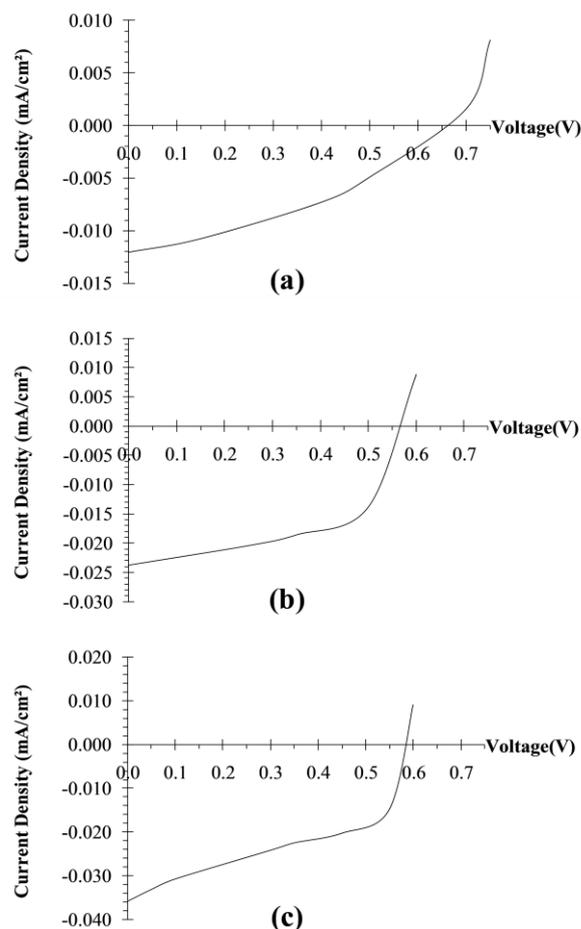
Fig. 7. J-V Curves of the fabricated solar cells using BTD with different weight ratios of (a) 0, (b) 5 and (c) 20 wt % showing threefold increase on the output power and J_{sc} and no noticeable change in the V_{oc}

Table 2. Characteristics of the fabricated solar cells

Active Layer	MEH-PPV:C_{60} (2:1)	MEH-PPV:C_{60} (2:1) + 5 wt % BTD	MEH-PPV:C_{60} (2:1) + 20 wt % BTD
J_{sc} (mA/cm^2)	-0.012	-0.024	-0.036
V_{oc} (V)	0.65	0.57	0.58
J_m (mA/cm^2)	-0.007	-0.014	-0.020
V_m (V)	0.4	0.5	0.45
P_m ($\mu W/cm^2$)	2.8	7.0	9.0
FF	0.36	0.51	0.43

5. Conclusion

In conclusion, the effect of BTD as a novel high mobility dopant with different weight ratios (0, 5 and 20 wt %) of the main active layer on photovoltaic performance of organic solar cells was investigated. This process was not continued to higher weight ratios to avoid significant composition change in the solar cells. The organic solar cells fabricated with classic low cost (low efficiency) materials, to clearly show the increase in output power and J_{sc}. The results showed that addition of BTD with 20 wt % of the main active layer had the best effect on the output power of the fabricated solar cells with threefold increase (from 2.8 to 9.0 $\mu W/cm^2$) (under an ordinary filament lamp) and the J_{sc} increased from 0.012 to 0.036 mA/cm^2, while the V_{oc} did not change noticeably. Considering the high electron mobility of BTD, the increased output power and J_{sc} resulted from the enhanced electron transportation by formation of such electron transport subnetworks. Furthermore, the surface roughness of the active layer decreased with increase in BTD weight ratios (0, 5 and 20 wt %). The smoother surface (i.e. more homogeneous morphology) may enhance the charge separation and transportation inside the device, resulting in higher interfacial current. In accordance with analytical models, this study practically suggests that a high mobility dopant such as BTD could be a promising active layer dopant to improve the efficiency of organic solar cells. This method is applicable to state of the art organic solar cells to improve the efficiency.

Acknowledgments

References

[1] B. Ratier, J. M. Nunzi, M. Aldissi, T. M Kraft, E. Buncel, Polym. Int. **61**(3), 342 (2012).

[2] G. Keru, P. G. Ndungu, V. O. Nyamori, Int. J. Energy Res. **38**(13), 1635 (2014).

[3] G. Li, V. Shrotriya, J. Huang, Y. Yao, T. Moriarty, K. Emery, Y. Yang, Nat. Mater. **4**, 864 (2005).

[4] M. Giulianini, E. R. Waclawik, J. M. Bell, M. Scarselli, P. Castrucci, M. De Crescenzi, N. Motta, Polymers **3**(3), 1433 (2011).

[5] B. Liu, W. L. Yu, Y. H. Lai, W. Huang, Chem. Mater. **13**(6), 1984 (2001).

[6] X. Zhang, S. A. Jenekhe, Macromolecules **33**(6), 2069 (2000).

[7] T. D. Nielsen, C. Cruickshank, S. Foged, J. Thorsen, F. C. Krebs, Sol. Energy Mater. Sol. Cells **94**(10), 1553 (2010).

[8] M. Helgesen, R. Søndergaard, F. C. Krebs, J. Mater. Chem. **20**, 36 (2010).

[9] D. M. Guldi, V. Sgobba, Chem. Commun. **47**, 606 (2011).

[10] G. Dennler, M. C. Scharber, C. J. Brabec, Adv. Mater. **21**(13), 1323 (2009).

[11] J. Roncali, Acc. Chem. Res. **42**(11), 1719 (2009).

[12] S. Liu, P. You, J. Li, J. Li, C. S. Lee, B. S. Ong, C. Surya, F. Yan, Energy Environ. Sci. **8**(5), 1463 (2015).

[13] J. M. Lee, J. S. Park, S. H. Lee, H. Kim, S. Yoo, S. O. Kim, Adv. Mater. **23**(5), 629 (2011).

[14] L. Lu, T. Xu, W. Chen, J. M. Lee, Z. Luo, I. H. Jung, H. I. Park, S. O. Kim, L. Yu, Nano Lett. **13**(6), 2365 (2013).

[15] L. Lu, T. Xu, W. Chen, E. S. Landry, L. Yu, Nat. Photonics **8**, 716 (2014).

[16] F. Machui, S. Rathgeber, N. Li, T. Ameri, C. J. Brabec, J. Mater. Chem. **22**(31), 15570 (2012).

[17] J. Lee, M. H. Yun, J. Kim, J. Y. Kim, C. Yang, Macromol. Rapid Commun. **33**(2), 140 (2012).

[18] Y. Zhang, D. Deng, K. Lu, J. Zhang, B. Xia, Y. Zhao, J. Fang, Z. Wei, Adv. Mater. **27**(6), 1071 (2015).

[19] B. A. D. Neto, A. A. M. Lapis, E. N. da Silva Júnior, J. Dupont, Eur. J. Org. Chem. **2013**(2), 228 (2013).

[20] P. Anant, N. T. Lucas, J. Jacob, Org. Lett. **10**(24), 5533 (2008).

[21] M. Watanabe, K. Goto, M. Shibahara, T. Shinmyozu, J. Org. Chem. **75**(18), 6104 (2010).

[22] K. M. Omer, S. Y. Ku, K. T. Wong, A. J. Bard, J. Am. Chem. Soc. **131**(30), 10733 (2009).

[23] K. D. Seo, I. T. Choi, Y. G. Park, S. Kang, J. Y. Lee, H. K. Kim, Dyes Pigm. **94**(3), 469 (2012).

[24] D. Jana, B. K. Ghorai, Tetrahedron Lett. **53**(14), 1798 (2012).

[25] L. Chen, L. Wang, X. Jing, F. Wang, J. Mater. Chem. **21**(28), 10265 (2011).

[26] A. Mishra, P. Bäuerle, Angew. Chem. **124**(9), 2060 (2012).

[27] A. Mishra, P. Bäuerle, Angew. Chem. Int. Ed. **51**(9), 2020 (2012).

[28] Y. M. Sun, G. C. Welch, W. L. Leong, C. J. Takacs, G. C. Bazan, A. J. Heeger, Nat. Mater. **11**(1), 44 (2012).

[29] Y. H. Chen, L. Y. Lin, C. W. Lu, F. Lin, Z. Y. Huang, H. W. Lin, P. H. Wang, Y. H. Liu, K. T. Wong, J. Wen, D. J. Miller, S. B. Darling, J. Am. Chem. Soc. **134**(33), 13616 (2012).

[30] L. Yang, J. K. Feng, A. M. Ren, J. Mol. Struct. Theochem. **816**(1-3), 161 (2007).

[31] M. Mohsennia, M. Massah Bidgoli, F. Akbari Boroumand, A. Mohsen Nia, Mater. Sci. Eng. B **197**, 25 (2015).

[32] T. Uemura, Y. Hirose, M. Uno, K. Takimiya, J. Takeya, Appl. Phys. Express **2**(11), 111501 (2009).

[33] A. Y. Amin, A. Khassanov, K. Reuter, T. Meyer-Friedrichsen, M. Halik, J. Am. Chem. Soc. **134**(40), 16548 (2012).

[34] J. J.-A. Chen, T. L. Chen, BS Kim, D. A. Poulsen, J. L. Mynar, J. M. J. Fréchet, B. Ma, ACS Appl. Mater. Interfaces **2** (9), 2679 (2010).

[35] S. Changsarn, R. Traiphol, T. Pattanatornchai, T. Srikhirin, P. Supaphol, J. Polym. Sci. B **47**(7), 696 (2009).

[36] J. Wang, Z. Li, S. Li, W. Qi, P. Liu, F. Liu, Y. Ye, L. Wu, L. Wang, W. Wu, PLoS ONE **8**(8), 1 (2013).

[37] U. Dettinger, H. J. Egelhaaf, C. J. Brabec, F. Latteyer, H. Peisert, T. Chassé, Chem. Mater. **27**(7), 2299 (2015).

[38] S. H. Yang, C. F. Lee, Optoelectron. Adv. Mat. **1**(4), 162 (2007).

[39] H. Kim, J. Y. Kim, K. Lee, H. Suh, Curr. Appl. Phys. **1**, 139 (2001).

[40] S. Zhang, L. Ye, W. Zhao, B. Yang, Q. Wang, J. Hou, Sci. China Chem. **58**, 248 (2015).

[41] E. S. Gadelmawla, M. M. Koura, T. M. A. Maksoud, I. Elewa, H. Soliman, J. Mater. Process. Technol. **123**, 133 (2002).

[42] G. Li, V. Shrotriya, Y. Yao, Y. Yang, J. Appl. Phys. **98**, 043704 (2005).

[43] U. Wurfel, D. Neher, A. Spies, S. Albrecht, Nat. Commun. **6**(6951), 1 (2015).

[44] J. T. Shieh, C. H. Liu, H. F. Meng, S. R. Tseng, Y. C. Chao, S. F. Horng, J. Appl. Phys. **107**, 084503 (2010).

[45] R. A. Street, Appl. Phys. Lett. **93**, 133308 (2008).

[46] F. Arabpour Roghabadi, K. Oniy Aghmiuni, V. Ahmadi, Org. Electron. **34**, 164 (2016).

_____

[*]Corresponding author: Boroumand@eetd.kntu.ac.ir